ChemComm

Detection of a Transient $Fe^{V}(O)(OH)$ Species Involved in Olefin Oxidation by a Bio-Inspired Non-Haem Iron Catalyst

Journal:	*ChemComm*
Manuscript ID	CC-COM-05-2018-003990.R1
Article Type:	Communication

Journal Name

COMMUNICATION

Detection of a Transient $Fe^{V}(O)(OH)$ Species Involved in Olefin Oxidation by a Bio-Inspired Non-Haem Iron Catalyst

Received 00th January 20xx,
Accepted 00th January 20xx

DOI: 10.1039/x0xx00000x

www.rsc.org/

Shuangning Xu,[a] Jedidiah J. Veach,[b] Williamson N. Oloo,[a] Kevin C. Peters,[b] Junyi Wang,[a] Richard H. Perry,[b,c*] and Lawrence Que, Jr.[a,*]

The iron tris(2-pyridylmethyl)amine) (Fe(TPA)) class of non-haem Fe catalysts is proposed to carry out selective hydrocarbon oxidations through the generation of high-valent Fe species. Using ambient mass spectrometry, we obtain direct evidence for the formation of an $Fe^{V}(O)(OH)$ species under catalytic conditions. In addition, ^{18}O-labelling suggests that this $Fe^{V}(O)(OH)$ species serves as the active oxidant in hydrocarbon oxidation catalysis.

Mononuclear non-haem iron-containing enzymes activate dioxygen to carry out a range of metabolically important transformations,[1-4,5] A common feature found for these enzymes is a mononuclear iron centre coordinated to a 2-His-1-carboxylate facial triad motif,[1] with two adjacent labile sites available for dioxygen binding and activation.[6, 7] Inspired by these enzymes, a class of non-haem iron catalysts has emerged, which are supported by tetradentate nitrogen-rich ligand frameworks such as TPA (TPA = tris(2-pyridylmethyl)amine) (Fig. 1 left) and use H_2O_2 as a two-electron oxidant to carry out stereoselective hydroxylation of C–H bonds, epoxidation of olefins, and *cis*-dihydroxylation of C=C bonds.[8-11] The high selectivity exhibited by these catalysts excludes unselective hydroxyl radicals as the oxidant but instead implicates metal-based oxidants, analogous to those proposed for metalloenzymes.

One important mechanistic question is the identity of the active oxidant. Significant evidence has been accumulated in the last 20 years from ^{18}O-labelling experiments to provide strong but indirect support for an Fe^{V} active oxidant in these catalytic systems (Fig. 1 right).[12-16] In our current understanding, an Fe^{II} precursor reacts with H_2O_2 to form a well-characterized metastable $Fe^{III}(OOH)$ species,[17, 18] which is a "sluggish oxidant" and does not oxidize substrates directly.[19] It is instead proposed to undergo rate-determining water-assisted O–O cleavage through a five-membered ring transition state (A in Fig. 1) to unmask an $Fe^{V}(O)$ oxidant (B in Fig. 1) responsible for the oxidative transformations associated with this catalyst.[13,14]

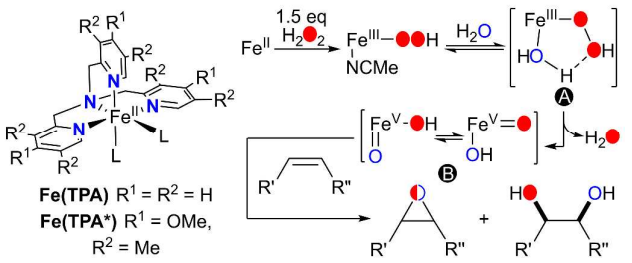

Figure 1. Iron complexes used in this study (left) and scheme showing the proposed water-assisted mechanism for Fe(TPA)-catalysed olefin oxidation by generation of a high-valent $Fe^{V}(O)(OH)$ species as the active oxidant (right).

Upon O–O bond cleavage, the distal oxygen atom from the $Fe^{III}(OOH)$ species is lost as water to generate the $Fe^{V}(O)(OH)$ oxidant with one O atom from H_2O_2 and the other O atom from water. This mechanism is supported by ^{18}O-labelling experiments showing partial incorporation of ^{18}O from $H_2{}^{18}O$ into alcohol and epoxide products, and the incorporation of one O atom from H_2O_2 and H_2O each into *cis*-diol products. The observed label incorporation can only occur after O–O bond cleavage to generate $Fe^{V}(O)(OH)$ followed by oxo-hydroxo tautomerism to scramble the isotopic labels (B in Fig. 1). As a result, the oxo oxygen that ends up in the alcohol or epoxide product could originate from either H_2O and H_2O_2.[13] On the other hand, olefin *cis*-dihydroxylation entails transfer of both the oxo and hydroxo groups of the $Fe^{V}(O)(OH)$ oxidant to the same face of the substrate C=C bond to form *cis*-diol with one oxygen atom each from H_2O and H_2O_2.[13]

There is scant direct spectroscopic evidence for such an $Fe^{V}(O)(OH)$ species in the literature, with only one report, by Costas and co-workers, on a related non-haem iron catalyst Fe(PyTACN) (PyTACN = 1-[2'-(pyridyl)methyl]-4,7-dialkyl-1,4,7-triazacyclononane). The $Fe^{V}(O)(OH)$ species was trapped and

[a] *Department of Chemistry and Center for Metals in Biocatalysis, University of Minnesota, Minneapolis, Minnesota 55455, United States. E-mail: larryque@umn.edu*
[b] *Department of Chemistry, University of Illinois, Urbana, IL 61801 (Previous affiliation for Richard H. Perry* where the work described herein was performed.*}*
[c] *Department of Chemistry and Physics, Nova Southeastern University, Fort Lauderdale, FL 33314. E-mail: richard.perry@nova.edu* (Current affiliation).
†Electronic Supplementary Information (ESI) available: [details of any supplementary information available should be included here]. See DOI: 10.1039/x0xx00000x

identified at -40 °C using cryo-spray ionization mass spectrometry (CSI-MS).[20] The transient nature of this Fe^{V} species under catalytic conditions presents a major challenge in obtaining direct evidence for its existence.

Desorption electrospray ionization MS (DESI-MS),[21, 22] the original ambient-ionization technique, enables direct analysis without the need for prior sample preparation or treatment[23] and is capable of detecting transient intermediates formed in catalytic reactions.[24-26] In these experiments, sensitivity is significantly influenced by microdroplet spray distances and angles relative to the sample surface and MS inlet. Transmission mode DESI (TM-DESI)[27, 28] reduces these optimisation requirements by directing the microdroplet sprayer at the MS inlet and using a mesh positioned perpendicular to the primary microdroplet beam as the sample surface. By placing reagents in the primary microdroplet spray and on mesh surfaces (Fig. 2), an ambient mass spectrometric technique[21] named multistage reactive TM-DESI (*r*TM^{n}-DESI,[24, 25] with *n* representing the number of desorption and/or reaction steps) offers a simple approach for detecting intermediates and products on a timescale < 1 ms. In addition, *r*TM^{n}-DESI provides the ability to spatially separate reagents and control their order of introduction into the reacting system, thereby minimizing unwanted reactions that lead to catalyst deactivation and degradation products.[25]

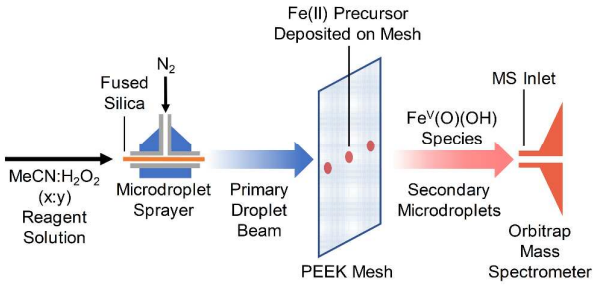

Figure 2. Experimental setup of *r*TM^{n}-DESI-MS, where ^{n} = 1.

This report describes *r*TM^{1}-DESI and ^{18}O labelling experiments that provide evidence for the formation of an $Fe^{V}(O)(OH)$ species under catalytic conditions and its involvement in substrate oxidation. In *r*TM^{1}-DESI-MS, a microdroplet spray containing MeCN and H_2O_2 impacts (velocity of the microdroplets ~ 50–100 m/s) a polyether ether ketone (PEEK) mesh (71 µm strand diameter, 56% open area) on which the iron complex $[Fe(TPA)(MeCN)_2](OTf)_2$ or $[Fe(TPA^*)(MeCN)_2](OTf)_2$ was deposited (5 µL of 1 mM solution in MeCN). When microdroplets impact the surface of the mesh, the iron complex is solubilized and desorbed into secondary microdroplets. The reaction of the iron complex with H_2O_2 proceeds in the secondary microdroplets, generating high-valent iron species that are detected using an Orbitrap mass spectrometer (mass accuracy 1-2 ppm and resolution of 100,000 at *m/z* 400[29]). The short timescale of desorption and microdroplet evaporation in *r*TM^{n}-DESI (< 1 ms) enabled detection of the $Fe^{V}(O)(OH)$ oxidant generated in the secondary microdroplets.

We first present results from the reactions of H_2O_2 with an electron-rich variant of Fe(TPA), namely Fe(TPA*) (TPA* = tris(3,5-dimethyl-4-methoxypyridyl-2-methyl)amine), with the expectation that TPA* should lengthen the lifetimes of the higher-valent species formed and enhance the intensities of these ions. With $H_2{}^{16}O_2$ and $H_2{}^{16}O$ in the reaction mixture (Fig. 3a), signals were observed at *m/z* 276.605, which can be formulated as either $[Fe^{III}(TPA^*)(^{16}O^{16}OH)]^{2+}$ or $[Fe^{V}(TPA^*)(^{16}O)(^{16}OH)]^{2+}$, and at *m/z* 702.163, which is consistent with either $\{[Fe^{III}(TPA^*)(^{16}O^{16}OH)](OTf)\}^{+}$ or $\{[Fe^{V}(TPA^*)(^{16}O)(^{16}OH)](OTf)\}^{+}$. A signal at *m/z* 704.133, arising from $[Fe^{III}(TPA^*)Cl(OTf)]^{+}$, was also observed, at around half the intensities of the $Fe^{III}(OOH)$ and/or $Fe^{V}(O)(OH)$ species (*m/z* 276.605: *m/z* 702.163: *m/z* 704.133 = 44:38:18). Signals of the ferrous precursor, ferric by-products as well as ferrous and ferric species with varying degrees of ligand oxidation were also observed (Table 1, Fig. S1).

Table 1. Iron species observed in *r*TM^{1}-DESI-MS experiments with unlabelled H_2O_2/H_2O.

Species	Dication (*m/z*)	Monocation with OTf (*m/z*)
$(L)Fe^{III}(OOH)$ or $(L)Fe^{V}(O)(OH)$	276.605 *189.543*	702.163 *528.038*
$(L)(Fe^{II})$	260.106	669.165
$(L)Fe^{III}(OH)$	268.608	686.168
$(L)Fe^{III}(Cl)$	-	704.133
$[(L)_2Fe^{III}{}_2(O)(OH)](OTf)$	611.188	-
$[(L)_2Fe^{III}{}_2(O)](OTf)_2$	677.163	-
$-CH_2-$ backbone hydroxylation	268.104	685.160
$(L)Fe^{III}(OH)$ w/ one $-CH_2-$ backbone oxidized to C=O	275.597	700.147

L = TPA*. Italicised number: *m/z* for corresponding species found when L = TPA.

When $H_2{}^{18}O_2$ was used (Fig. 3b), base peaks at *m/z* 277.607 and *m/z* 704.167, corresponding to $Fe^{V}(O)(OH)$ species with single ^{18}O atom incorporation, were observed. The absence of appreciable signals at *m/z* 278.608 and *m/z* 706.171 indicates that single ^{18}O substitution predominates, thereby excluding the $Fe^{III}(OOH)$ species, which would carry both ^{18}O atoms from $H_2{}^{18}O_2$. These observations support a mechanism involving water-assisted O–O bond cleavage of $Fe^{III}(OOH)$ species to form $[Fe^{V}(TPA^*)(^{16}O)(^{18}OH)]^{2+}$ or $[Fe^{V}(TPA^*)(^{18}O)(^{16}OH)]^{2+}$ (Fig. 1). The *r*TM^{1}-DESI-MS results are in congruence with previous bulk-phase ^{18}O-labelling studies for alcohol, epoxide, and *cis*-diol products of these reactions.[12-16] Complementary $H_2{}^{16}O_2/H_2{}^{18}O$ experiments (Fig. 3c) also saw an increase in the relative intensities of *m/z* 277.607 and *m/z* 704.167 peaks compared to the reaction with $H_2{}^{16}O_2/H_2{}^{16}O$, suggesting ^{18}O-atom incorporation from $H_2{}^{18}O$. The peak at *m/z* 704.133 present in the $H_2{}^{16}O_2/H_2{}^{16}O$ experiment and assigned to $[Fe^{III}(TPA^*)Cl(OTf)]^{+}$ can be clearly resolved from the *m/z* 704.167 peak arising from single ^{18}O-labelled $Fe^{V}(O)(OH)$ species (Fig 3a and 3c insets). The signals attributed to ligand degradation products in Table 1 were insensitive to isotopic labelling and saw no significant changes in relative intensities,

suggesting that these pre-existing impurities did not participate in these reactions (Fig. 3, Fig. S2).

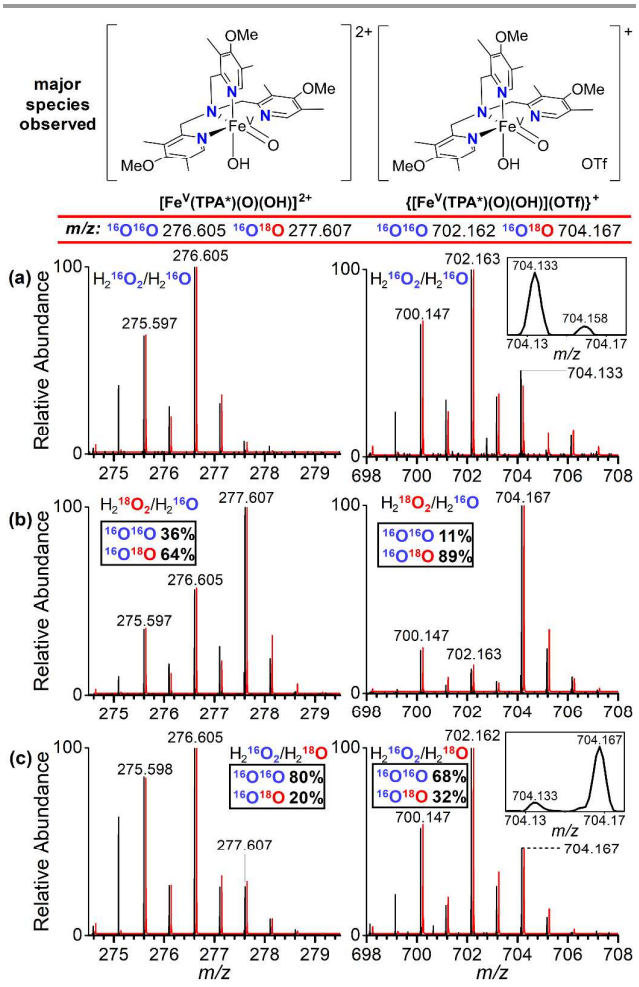

Figure 3. Mass spectra (*r*TM^1-DESI-MS) of reaction mixtures of Fe^{II}(TPA*) with spray mixtures containing isotopically labelled H_2O and H_2O_2. (a) 15 mM 90% $H_2{}^{16}O_2$ in $H_2{}^{16}O$; (b) 120 μM $H_2{}^{18}O_2$ (2% in $H_2{}^{16}O$, 90% ^{18}O enriched) in MeCN; (c) 20 mM 90% $H_2{}^{18}O_2$/0.5 M $H_2{}^{18}O$ in MeCN. Insets: zoomed in region of spectra. *m/z* ratios shown underneath the formulae are the expected *m/z* ratios Offset Red traces are simulated spectra of the corresponding mixture of ions computed using Thermo Xcalibur (see Fig. S3 for parameters for the simulations).

Parallel experiments on the parent Fe^{II}(TPA) complex corroborate the results observed for Fe^{II}(TPA*) (Fig. S4). Signals at *m/z* 190.545 and *m/z* 530.043, consistent with the incorporation of a single ^{18}O-atom into the Fe^{V}(O)(OH) species are observed for the $H_2{}^{18}O_2/H_2{}^{16}O$ reaction, along with signals at *m/z* 191.547 and *m/z* 532.047, consistent with Fe^{III}(OOH) species with both oxygen atoms of the peroxo moiety originating from H_2O_2. Interestingly, while the relative intensity of the Fe^{V}(O)(OH) dication (*m/z* 189.543) is 4 times that of penta-coordinated Fe^{III}(OOH) dication (*m/z* 191.547), the triflate-bound Fe^{III}(OOH) species (*m/z* 532.047) [Fe^{III}(TPA)($^{18}O^{18}$OH)(OTf)]$^+$ dominates the *m/z* 530 region and is about 9 times the intensity of the corresponding triflate-bound Fe^{V}(O)(OH) species (*m/z* 530.043). This drastic difference in speciation suggests triflate coordination to the sixth site of the Fe^{III}(OOH) species, which prevents water-assisted O–O bond cleavage in the gas phase and leads to the accumulation of the Fe^{III}(OOH) species. Indeed, under the conditions of these experiments, the use of the $H_2{}^{16}O_2/H_2{}^{18}O$ combination did not result in the appearance of the Fe^{V}(O)(OH) species with a single ^{18}O atom incorporated and major species observed were consistent with Fe^{III}($^{16}O^{16}$OH) species.

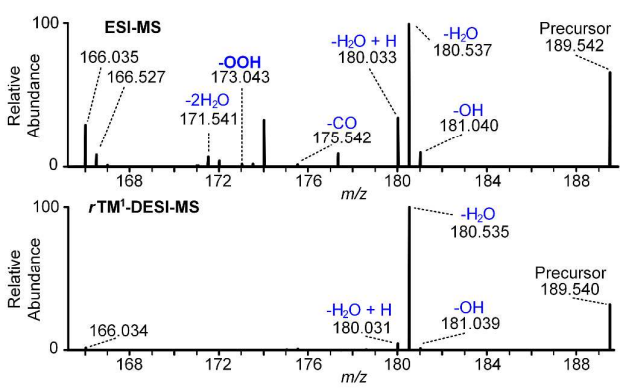

Figure 4 Tandem mass spectra (30% normalized collision energy) of *m/z* 189.542 in *r*TM^1-DESI-MS (top) and ESI-MS (bottom). Reactions conditions for ESI-MS: 0.7 mM Fe^{II}(TPA) and 7 mM $H_2{}^{18}O_2$ in MeCN were infused into a mixing tee (-40 °C) at 4 μL/min. The reaction mixture was then infused into an ESI source with 60 psi nebulizing gas; the resulting reaction time was approximately 4 seconds.

Further insight was obtained from tandem mass spectrometry (MS/MS) experiments (Fig. 4). Using cold mixing-tee electrospray ionization mass spectrometry (ESI-MS), the ion at *m/z* 189.542 dissociates to yield fragments at *m/z* 181.040, *m/z* 180.537, *m/z* 180.033, and *m/z* 173.043, which correspond to loss of OH (17 Da), H_2O (18 Da), [H_2O + H] (19 Da) and OOH (33 Da), respectively. On the other hand, fragmentation of the species at *m/z* 189.540 in *r*TM^1-DESI-MS affords three peaks at *m/z* 181.039, m/z 180.535, and *m/z* 180.031 corresponding to the loss of OH (17 Da), H_2O (18 Da), and [H_2O + H] (19 Da), respectively, with different relative intensities compared to those obtained from ESI-MS. In addition, the loss of OOH (33 Da) is not observed in *r*TM^1-DESI MS/MS experiments. These observations indicate that the ion populations at *m/z* 189.542 in ESI-MS and *r*TM^1-DESI-MS correspond to species with different chemical structures and/or compositions.

The signal at *m/z* 189.540 can be formulated as either [Fe^{III}(TPA)($^{16}O^{16}$OH)]$^{2+}$ or [Fe^{V}(TPA)(^{16}O)(^{16}OH)]$^{2+}$. The intensity of the parent ion signal at *m/z* 189.540 relative to the fragment peak at *m/z* 180.535 (-H_2O) in the MS/MS spectra is much higher for ESI-MS (≈50 ± 17%) than for *r*TM^1-DESI (≈17 ± 11%) (average for multiple experiments; Fig. 4 shows one set of spectra). The lower ratio observed in the *r*TM^1-DESI experiment is most likely due to facile loss of •OH from Fe^{V}(O)(OH) rather than from Fe^{III}(OOH), owing to the stronger O–O bond in the hydroperoxo species than the Fe^{V}–OH bond in its isomer. The nascent •OH then abstracts a H-atom from the ligand to form H_2O. Ligand oxidation during catalysis has been ruled out by control experiments that evaluated the reaction of free TPA ligand with H_2O_2 and Fe(TPA) (Fig. S5). In these experiments, free TPA ligand and Fe(TPA) were deposited on a series of meshes (*r*TM^2-DESI-MS). When the microdroplet spray containing H_2O_2 reacted with free TPA

ligand (mesh 2) and Fe(TPA) (mesh 1), ion signals corresponding to ligand oxidation products were not observed (Fig. S5). In addition to the facile loss of •OH observed in the *r*TM^1-DESI spectra, the absence of a signal at *m/z* 173.043 due to loss of OOH also supports the notion that the parent ion at *m/z* 189.540 is primarily composed of the $[Fe^V(TPA)(O)(OH)]^{2+}$ ion; the same argument would apply to the ion population at *m/z* 276.605, which would primarily be composed of $[Fe(TPA^*)(O)(OH)]^{2+}$. Detection of the highly reactive $Fe^V(O)(OH)$ intermediate by *r*TM^1-DESI is enabled by the short timescales for desorption, reagent transfer, and evaporation of the secondary microdroplets in *r*TM^n-DESI (< 1 ms). In contrast, the reaction times for the ESI-MS experiments using a cold mixing tee (-40 ^{o}C) are on the order of a few seconds, resulting in lower yields and/or complete depletion of the $Fe^V(O)(OH)$ moiety prior to analysis.

In an attempt to observe oxygenated products directly, substrate oxidation experiments with a *r*TM^1-DESI setup were carried out in which a solution of 4-vinylaniline (4VA):H_2O_2 was sprayed onto a mesh that was bare (Fig. S6a) or one that contained Fe(TPA) (Fig. S6b). As shown in Fig. S6a, peaks at *m/z* 120.081 and *m/z* 136.076 were observed, corresponding to $[4VA + H]^+$ and its protonated oxidized product formed from reaction with H_2O_2, respectively. When Fe(TPA) was added to the mesh (Fig. S6b), the product-to-substrate ratio increased by at least a factor of ten. The identity of the peak at *m/z* 136 was confirmed using MS/MS (Fig. S6c), which showed a fragmentation pattern indicating oxygenation of the C=C bond. These results show that catalytic conversion occurs on the *r*TM^n-DESI timescale and strongly implicate the Fe-based intermediates observed by *r*TM^n-DESI during catalysis.

In conclusion, we have reported evidence for the formation of an $Fe^V(O)(OH)$ species in the reactions of a bio-inspired non-haem iron catalysts Fe(TPA) and Fe(TPA*) (a more electron-rich variant of TPA) with H_2O_2. The short timescales for desorption and microdroplet evaporation in *r*TM^n-DESI-MS have enabled detection of this transient catalytic intermediate under ambient conditions. The identity of the $Fe^V(O)(OH)$ oxidant was established experimentally using ^{18}O-labelled H_2O_2 and H_2O experiments. This work identifies directly the proposed iron intermediate active in Fe(TPA)-catalysed hydrocarbon oxidations.

Acknowledgments

The University of Illinois at Urbana-Champaign (UIUC) provided financial support (the work described in this article was completed at UIUC and in collaboration with colleagues at the University of Minnesota). The work at the University of Minnesota (UMN) was supported by the US Department of Energy, Office of Basic Energy Sciences (Grant DE-FG02-03ER15455 to L.Q.). We also acknowledge the staff of the mass spectrometry facility in the UMN Masonic Cancer Center for access to instrumentation.

Notes and References

1. S. Kal and L. Que, Jr., *J. Biol. Inorg. Chem.*, 2017, **22**, 339-365.
2. J. Serrano-Plana, A. Company and M. Costas, in *Adv. Inorg. Chem.*, eds. R. van Eldik and C. D. Hubbard, Academic Press, 2017, vol. 70, pp. 63-105.
3. E. G. Kovaleva and J. D. Lipscomb, *Nat. Chem. Biol.*, 2008, **4**, 186.
4. M. D. White and E. Flashman, *Curr. Opin. Chem. Biol.*, 2016, **31**, 126-135.
5. S. M. Barry and G. L. Challis, *ACS Catalysis*, 2013, **3**, 2362-2370.
6. A. Karlsson, J. V. Parales, R. E. Parales, D. T. Gibson, H. Eklund and S. Ramaswamy, *Science*, 2003, **299**, 1039-1042.
7. B. M. Martins, T. Svetlitchnaia and H. Dobbek, *Structure*, 2005, **13**, 817-824.
8. G. Olivo, O. Cussó, M. Borrell and M. Costas, *J. Biol. Inorg. Chem.*, 2017, **22**, 425-452.
9. W. N. Oloo and L. Que, Jr., *Acc. Chem. Res.*, 2015, **48**, 2612-2621.
10. K. P. Bryliakov and E. P. Talsi, *Coord. Chem. Rev.*, 2014, **276**, 73-96.
11. M. C. White, *Science*, 2012, **335**, 807-809.
12. K. Chen and L. Que, Jr., *J. Am. Chem. Soc.*, 2001, **123**, 6327-6337.
13. K. Chen, M. Costas, J. Kim, A. K. Tipton and L. Que, Jr., *J. Am. Chem. Soc.*, 2002, **124**, 3026-3035.
14. W. N. Oloo, A. J. Fielding and L. Que, Jr., *J. Am. Chem. Soc.*, 2013, **135**, 6438-6441.
15. A. Company, L. Gomez, M. Guell, X. Ribas, J. M. Luis, L. Que, Jr. and M. Costas, *J. Am. Chem. Soc.*, 2007, **129**, 15766-15767.
16. A. Company, Y. Feng, M. Güell, X. Ribas, J. M. Luis, L. Que, Jr. and M. Costas, *Chem. Eur. J.*, 2009, **15**, 3359-3362.
17. R. Y. N. Ho, G. Roelfes, B. L. Feringa and L. Que, Jr., *J. Am. Chem. Soc.*, 1999, **121**, 264-265.
18. M. Costas, M. P. Mehn, M. P. Jensen and L. Que, Jr., *Chem. Rev.*, 2004, **104**, 939-986.
19. M. J. Park, J. Lee, Y. Suh, J. Kim and W. Nam, *J. Am. Chem. Soc.*, 2006, **128**, 2630-2634.
20. I. Prat, J. S. Mathieson, M. Guell, X. Ribas, J. M. Luis, L. Cronin and M. Costas, *Nat. Chem.*, 2011, **3**, 788-793.
21. R. G. Cooks, Z. Ouyang, Z. Takats and J. M. Wiseman, *Science*, 2006, **311**, 1566-1570.
22. Z. Takats, I. Cotte-Rodriguez, N. Talaty, H. Chen and R. G. Cooks, *Chem. Commun.*, 2005, 1950-1952.
23. D. R. Ifa, C. Wu, Z. Ouyang and R. G. Cooks, *Analyst*, 2010, **135**, 669-681.
24. R. H. Perry, K. R. Brownell, K. Chingin, T. J. Cahill, R. M. Waymouth and R. N. Zare, *Proc. Natl. Acad. Sci. U.S.A.*, 2012, **109**, 2246-2250.
25. R. H. Perry, T. J. Cahill, J. L. Roizen, J. Du Bois and R. N. Zare, *Proc. Natl. Acad. Sci. U.S.A.*, 2012, **109**, 18295-18299.
26. R. H. Perry, M. Splendore, A. Chien, N. K. Davis and R. N. Zare, *Angew. Chem., Int. Ed.*, 2011, **50**, 250-254.
27. J. E. Chipuk and J. S. Brodbelt, *J. Am. Soc. Mass Spectrom.*, 2008, **19**, 1612-1620.
28. J. J. Perez, G. A. Harris, J. E. Chipuk, J. S. Brodbelt, M. D. Green, C. Y. Hampton and F. M. Fernandez, *Analyst*, 2010, **135**, 712-719.
29. R. H. Perry, R. G. Cooks and R. J. Noll, *Mass Spectrom. Rev.*, 2008, **27**, 661-699.

TOC Graphics

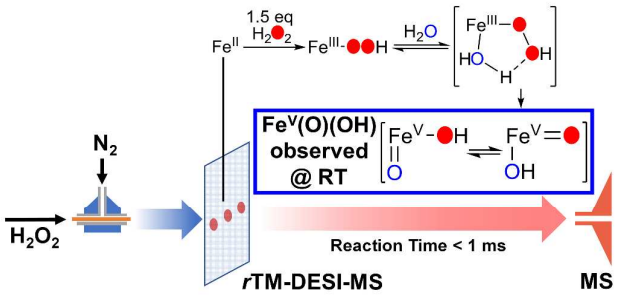

Here we provide direct evidence for the formation of an $Fe^{V}(O)(OH)$ species in non-haem iron catalysis by using an ambient mass spectrometric technique.